Design and Analysis of CMOS-Based Terahertz Integrated Circuits by Causal Fractional-Order RLGC Transmission Line Model

Yang Shang, *Student Member, IEEE*, Hao Yu, *Member, IEEE*, and Wei Fei, *Student Member, IEEE*

***Abstract*—A causal and compact fractional-order model is developed for complementary metal–oxide–semiconductor (CMOS) on-chip transmission line (T-line) at Terahertz (THz) frequencies. With consideration of the loss from frequency-dependent dispersion and nonquasi-static effects at THz, good agreement of characteristic impedance is observed between the proposed fractional-order model and the measurement up to 110 GHz, while traditional integer-order model can only match up to 10 GHz. The developed fractional-order model is further deployed in the design and analysis of CMOS-based THz integrated circuits that utilize T-line, such as standing-wave oscillator, which has significantly improved accuracy with causality.**

***Index Terms*—Causality, fractional-order, terahertz, transmission-line model.**

I. Introduction

THE APPLICATIONS in terahertz (THz) frequency region (0.1–10 THz) are able to fill the gap between electronics and photonics. As it has large propagation loss by molecular absorption for long-range applications, THz has wide applications in short-range communication and imaging due to big-data bandwidth and high detection sensitivity [1]. For example, THz signal is very sensitive to the composition of human tissue, which can result in new millimeter-wave imaging systems for biomedical diagnosis. Recent researches have shown successful revelation of contrast in THz images of skin and breast cancer [2]. At the same time, the advance scaling of complementary metal–oxide–semiconductor (CMOS) technology has made it possible for designs at THz region with significantly improved cut-off frequency around 600 GHz at 22 nm. According to the International Technology Roadmap for Semiconductors (ITRS), the expected cut-off frequency of CMOS transistors is 0.9 THz in 2021. However, the primary challenge in CMOS based THz design is how to develop accurate device models that can take into account the loss from strong frequency-dependent dispersion and nonquasi-static effects in THz. As the most fundamental passive structure, the modeling of transmission line (T-line) in CMOS is under significant interest in various designs [3]–[12].

Manuscript received February 15, 2013; revised April 04, 2013; accepted June 10, 2013. Date of publication June 28, 2013; date of current version September 09, 2013. This work was supported by Singapore MOE Tier-1 funding RG 26/10. This paper was recommended by Guest Editor A. Elwakil.

The authors are with the School of Electrical and Electronic Engineering, Nanyang Technological University, 639798 Singapore (e-mail: haoyu@ntu.edu.sg).

Digital Object Identifier 10.1109/JETCAS.2013.2268948

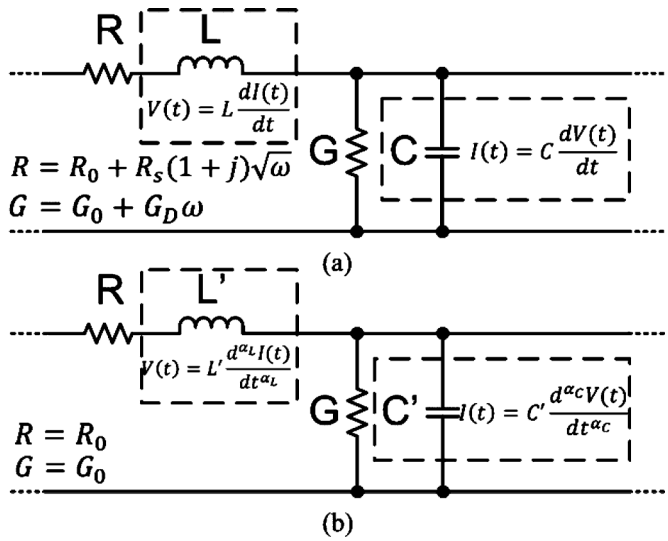

Fig. 1. RLGC unit-cell equivalent circuits of T-line: (a) integer-order model and (b) fractional-order model.

Traditionally, T-line is characterized by distributed integer-order RLGC model shown in Fig. 1(a) [13]. Drude's classical relaxation-effect model is deployed for the skin effect with R_s [14], [15]. In addition, the loss due to dielectric polarization and dipole rotation can be modeled by a dielectric-loss of G_D. However, such an integer-order model is insufficient to describe the T-line performance at THz region because the loss term in T-line is difficult to model the dispersion loss and nonquasi-static effects [16], which can cause large deviation at THz frequency region. Such impact is further verified by the measurement results and circuit level simulations in this paper. Moreover, traditional T-line model has causality issue. Physically, the real and imaginary parts of both permittivity $\varepsilon(\omega)$ and permeability $\mu(\omega)$ in a propagation medium are not independent to each other, but follow the Kramers–Kronig relation [17]. As such, the extracted RLCG parameters in traditional T-line model may result in a noncausal response in the model that can induce both accuracy and convergence problems in the time-domain simulation.

The concept of fractional-order model has been examined to model capacitor (C) and inductor (L) at high-frequency region. The I-V relation of a capacitor is found to follow the fractional-order [18], and the eddy current and hysteresis effect in inductors are also observed with fractional-order relation [19]. It motivates us to reexamine the RLCG T-line model at THz during the device characterization [20]. Note that fractional-

order model has been deployed to model the surface impedance [21] and describe the abnormal diffusion of voltage and current wave [22]. The fractional-order based impedance matching network [23], [24] and resonator design [25] have also been studied. However, no studies investigating the model causality have been carried on with measurement verifications at THz.

In this paper, we have developed a fractional-order RLGC model for T-line at THz with the following advantages. Firstly, the fractional-order RLGC model can describe dispersion and nonquasi-static effect in THz. Next, by properly deciding the range of fractional-order, the fractional-order model does not have the causality issue. Lastly, the fractional-order model is still in a compact RLGC form that can be extracted from measurement results. The proposed factional-ordered RLGC model is verified with S-parameter measurement results of T-lines from 10 MHz to 110 GHz. Compared to the conventional integer-order RLGC model, the proposed fractional-order RLGC model demonstrates improved accuracy of characteristic impedance and shows significant impact to THz circuit design.

The rest of this paper is organized as follows. Section II briefly reviews the calculation of fractional calculus, and the application to the fractional-order T-line model. The model extraction of fractional-order T-line and causality analysis are shown in Section III. The fractional-order model verification by measurement results are presented in Section IV. The fractional-order model applications in THz circuit designs are discussed in Section V. The paper is concluded in Section VI.

II. Fractional-Order Transmission Line Model

A. Fractional Calculus

Generally, most of dynamic systems can be described with fractional dynamics, though the fractionality is rather low to be considered than the integer-order behavior. Recently, the fractional-order models are re-examined when considering loss terms in many fields [26] including electronics [18], [19], [27] electromagnetic [28], fluidic-dynamics [29], material technology [30], quantum mechanics [31], etc.

Fractional calculus was initiated by a question of half-order derivative from *L' Hospital* in 1695 and was generalized by *Euler* in [32]. In fractional calculus, the integration and differentiation can be generalized by the operator ${}_aD_t^\alpha$ [33]

$$ {}_aD_t^\alpha = \begin{cases} \frac{d^\alpha}{dt^\alpha}, & \alpha > 0 \\ \int_a^t (d\tau)^\alpha, & \alpha < 0 \end{cases} \tag{1} $$

where α is a real number, and t and a are the lower and upper bounds. Note that differentiation and integration can be treated as the special cases when α equals 1 or -1, respectively.

By Riemann–Liouville definition, the operator ${}_aD_t^\alpha$ can be expressed by the following equation $(n-1 < \alpha < n)$:

$$ {}_aD_t^\alpha f(t) = \frac{1}{\Gamma(n-\alpha)} \frac{d^n}{dt^n} \int_a^t \frac{f(\tau)}{(t-\tau)^{\alpha-n+1}} d\tau \tag{2} $$

where $\Gamma(\cdot)$ is the Euler's gamma function.

Assuming the lower bound $a = -\infty$, one can take the Fourier transform of (2) to obtain the generalized expression of fractional integral in frequency domain for $0 < \alpha < 1$

$$ F\left\{ {}_{-\infty}D_t^{-\alpha} f(t) \right\} = (j\omega)^{-\alpha} G(\omega). \tag{3} $$

Similarly, the generalized expression of fractional derivative in frequency domain is

$$ F\{D^\alpha f(t)\} = (-j\omega)^\alpha G(\omega). \tag{4} $$

As shown in (3) and (4), the fractional-operator in frequency domain can be treated as the product of a magnitude scaling factor ω^α and a phase rotation factor $(j)^{-\alpha}$. Theoretically the physical behavior of any electronic device can be described by these two fractional factors. More importantly, both scaling factor and rotation factor are linked by a fractional-order α, which ensures the reality of one dynamic system with dissipation. Therefore, in order to examine the loss terms for electronic devices at THz, the aforementioned fractional calculus can be applied with many interesting observations as explored in the following sections.

B. Fractional-Order Capacitance and Inductance Models

In this paper, we show that fractional-order model for T-line can be built by introducing fractional-order terms in the conventional RLGC model as shown in Fig. 1(b). A fractional-order capacitor model [18] with the *I-V* relation can be given by

$$ I(t) = C' \frac{d^{\alpha_C} V(t)}{dt^{\alpha_C}} = C'_0 D_t^{\alpha_C} V(t) \tag{5} $$

where C' is the fractional capacitance with order α_C, and $\alpha_C \in (0, 1]$ is the fractional-order relating to the loss of capacitor.

Similarly, the I-V relation of fractional-order inductor [19] is

$$ V(t) = L' \frac{d^{\alpha_L} I(t)}{dt^{\alpha_L}} = L'_0 D_t^{\alpha_L} I(t) \tag{6} $$

where L' is the fractional inductance with order α_L, and $\alpha_L \in (0, 1]$ is the fractional-order relating to the loss of inductor.

The admittance and impedance of fractional-order capacitor and inductor can be obtained from (5) and (6) by

$$ Y'(\omega) = \omega^{\alpha_C} C' e^{\frac{j\alpha_C \pi}{2}} \tag{7} $$

$$ Z'(\omega) = \omega^{\alpha_L} L' e^{\frac{j\alpha_L \pi}{2}}. \tag{8} $$

When α_L *or* $\alpha_C \neq 1$, we can expect the existence of real-parts at the right-hand sides of (7) and (8), which represent the frequency-dependent loss. Physically in a particular device, the fractional-order operator indicates the transfer of the energy storage to energy loss. As such, the distributed frequency-dependent terms are considered by L' and C' elements in fractional-order terms.

C. Fractional-Order T-Line Model

Note that the fractional-order T-line can be analyzed in a similar fashion as to the traditional T-line. The characteristic impedance (Z_0) of T-line can be found by $\sqrt{Z/Y}$, where Z

and Y are the series impedance and shunt admittance, respectively. Based on (7) and (8) with consideration of resistance R_0 and conductance G_0, one can have

$$Z_0 = \sqrt{\left(R_0 + \omega^{\alpha_L} L' e^{\frac{j\alpha_L \pi}{2}}\right) \Big/ \left(G_0 + \omega^{\alpha_C} C' e^{\frac{j\alpha_C \pi}{2}}\right)}. \tag{9}$$

In THz frequency region, ω is in the order of $10^{11} - 10^{13}$. At such a high frequency, we have $R_0 \ll \omega^{\alpha_L} L' e^{(j\alpha_L \pi)/(2)}$ and $G_0 \ll \omega^{\alpha_C} C' e^{(j\alpha_C \pi)/(2)}$, so (9) can be approximated as

$$Z_0 = \sqrt{L'/C'} \cdot \omega^{\frac{\alpha_L - \alpha_C}{2}} \cdot \left[\cos\frac{(\alpha_L - \alpha_C)\pi}{4} + jsin\frac{(\alpha_L - \alpha_C)\pi}{4}\right]. \tag{10}$$

Comparing characteristic impedance by the fractional-order and the conventional integer-order RLGC models, one can observe that the fractional-order Z_0 has nonlinear frequency dependency in THz. If $\alpha_L < \alpha_C$, magnitude of Z_0 has an inverse-square-root-like decreasing function of frequency. This reveals the existence of imaginary part in Z_0, which accounts for the dispersion and nonquasi-static effects. Both effects are confirmed in the THz T-line measurements.

Moreover, the propagation constant (γ) is

$$\gamma = \alpha + j\beta \tag{11}$$

where α is the attenuation constant and β is the phase constant.

As $\gamma = \sqrt{ZY}$, with (7) and (8), one can have

$$\gamma = \sqrt{\left(R + \omega^{\alpha_L} L' e^{\frac{j\alpha_L \pi}{2}}\right)\left(G + \omega^{\alpha_C} C' e^{\frac{j\alpha_C \pi}{2}}\right)}. \tag{12}$$

In THz frequency region, since $R_0 \ll \omega^{\alpha_L} L' e^{(j\alpha_L \pi)/(2)}$ and $G_0 \ll \omega^{\alpha_C} C' e^{(j\alpha_C \pi)/(2)}$, (12) can be approximated as

$$\gamma = \sqrt{L'C'} \cdot \omega^{\frac{\alpha_L + \alpha_C}{2}} \cdot \left(\cos\frac{(\alpha_L + \alpha_C)\pi}{4} + jsin\frac{(\alpha_L + \alpha_C)\pi}{4}\right). \tag{13}$$

Comparing propagation constant by the fractional-order and the conventional integer-order RLGC models, one can observe that the fractional-order γ also has nonlinear frequency dependency in THz. The attenuation constant α will become nonzero when $\alpha_L + \alpha_C < 2$ in (13), and the energy loss is introduced accordingly.

What is more, note that the S-parameters of T-line are determined by Z_0 and γ [34]

$$\begin{bmatrix} S11 & S12 \\ S21 & S22 \end{bmatrix} = \begin{bmatrix} \frac{A+B/Z_0-CZ_0-D}{A+B/Z_0+CZ_0+D} & \frac{2(AD-BC)}{A+B/Z_0+CZ_0+D} \\ \frac{2}{A+B/Z_0+CZ_0+D} & \frac{-A+B/Z_0-CZ_0+D}{A+B/Z_0+CZ_0+D} \end{bmatrix} \tag{14}$$

where $\begin{bmatrix} A & B \\ C & D \end{bmatrix} = \begin{bmatrix} \cosh\gamma l & Z_0 \sinh\gamma l \\ \sinh\gamma l/Z_0 & \cosh\gamma l \end{bmatrix}$ is the transfer matrix of uniform T-line. By substituting (9) and (12) into (14), one can obtain the S-parameters of the fractional-order T-line model. As such, the models can be verified by the S-parameters measurement results.

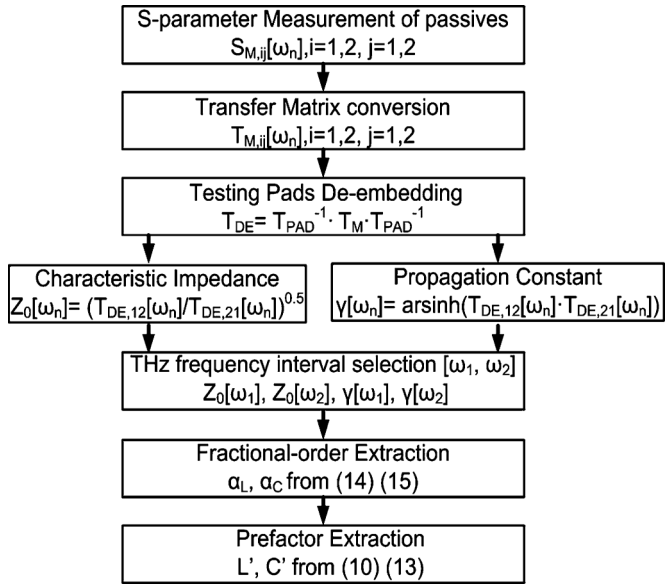

Fig. 2. Fractional-order T-line modeling parameters extraction flow.

In addition, it is well known that the propagation velocity of the EM wave front (V_p) equals to ω/β. In the fractional-order T-line model, one can have

$$V_P = \omega^{1-\frac{\alpha_L + \alpha_C}{2}} \Big/ \left(\sqrt{L'C'} \cdot \sin\frac{(\alpha_L + \alpha_C)\pi}{4}\right). \tag{15}$$

As such, one can have following observations. In the fractional-order T-line model, when $\alpha_L + \alpha_C < 2$ in (13), V_p becomes nonlinearly frequency dependent in high-frequency region like THz. This reveals dispersion effect when propagating through lossy media. On the other hand, in the integer-order T-line model, when $\alpha_L + \alpha_C = 2$ in (13), V_p equals $1/\sqrt{L'C'}$, which is not frequency dependent to model the dispersion effect in high-frequency region like THz.

III. Model Extraction and Causality Analysis

T-line is a passive, linear and time-invariant (LTI) network. The extracted T-line model is thereby needed to be causal. In this section, the extraction flow of fractional-order T-line model is introduced with the additional causality checking and enforcement followed by comparison with the traditional integer-order counterpart.

A. Fractional-Order Model Extraction

A fractional-order model parameters extraction flow for T-line at THz is illustrated in Fig. 2. The extraction begins with the measurement data obtained from a Vector Network Analyzer. Firstly, the measurement data is converted into transfer matrix (T matrix) for an easy operation, and the error terms contributed by the testing pads are removed by de-embedding process. Secondly, characteristic impedance Z_0 and propagation constant γ are calculated from de-embedded T-matrix according to [35]. Afterwards, one can define the modeling frequency interval $[\omega_1, \omega_2]$ in THz region based on his interests.

From (10), one can have

$$\alpha_L - \alpha_C = 2\log_{\left(\frac{\omega_1}{\omega_2}\right)} |Z_0(\omega_1)/Z_0(\omega_2)| \tag{16}$$

where $Z_0(\omega_1)$ and $Z_0(\omega_2)$ are the characteristic impedances at frequencies ω_1 and ω_2 in THz region, respectively.

From (13), one can have

$$\alpha_L + \alpha_C = 2\log_{\left(\frac{\omega_1}{\omega_2}\right)} |\gamma(\omega_1)/\gamma(\omega_2)| \tag{17}$$

where $\gamma(\omega_1)$ and $\gamma(\omega_2)$ are the propagation constants at frequencies ω_1 and ω_2 in THz region, respectively.

By combining (16) and (17), α_L and α_C can be obtained in the fractional-order model; and by substituting α_L and α_C into (10) and (13), fractional-order L' and C' can be obtained as well. Note that L' and C' are the p.u.l. (per-unit-length) prefactors with corresponding units of $\mathrm{Vs}^{-\alpha_\mathrm{L}}\mathrm{A}^{-1}$/m and $\mathrm{As}^{-\alpha_\mathrm{C}}\mathrm{V}^{-1}$/m, respectively, but not p.u.l. inductance and capacitance anymore.

Moreover, in order to apply the fractional-order T-line model in the time-domain simulator likes Cadence Spectre. The model needs to be converted from frequency domain into time-domain by rational functional approximation

$$f(s) \approx \sum_{j=1}^{N} \frac{c_j}{s - a_j} + d + sh. \tag{18}$$

Here, N is the rational order, a_j and c_j are the poles and residues in complex conjugate pairs, d and h are real. The coefficients in (18) can be obtained by vector fitting algorithm as introduced in [36]. Note that the error introduced by the frequency to time conversion is well controlled by increasing the rational-fitting order.

B. Causal LTI System and Causality Enforcement

To understand the causality for the extracted fractional-order T-line model, the fundamentals of causal LTI system are first reviewed here.

In a LTI system, the impulse response $h(t)$ to an input $x(t)$ can be expressed as [37]

$$y(t) = x(t) * h(t) = \int_{-\infty}^{+\infty} h(t-\tau)x(\tau)d\tau \tag{19}$$

where $x(t)$ and $y(t)$ represent the input and output voltages, currents, or powers of T-line network, and $h(t)$ is the corresponding admittance or impedance state matrix.

The principle of causality states that there is no effect happened before its cause. As such, a causal LTI system $h(t)$ can be mathematical defined as

$$h(t) = 0, \forall t < 0. \tag{20}$$

The causality of T-line model can be verified by this definition in time-domain. Equation (20) can be equivalently represented as

$$h(t) = sign(t)h(t) \tag{21}$$

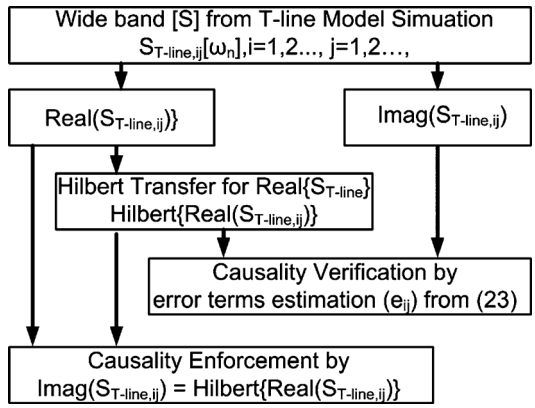

Fig. 3. Causality verification and enforcement flow.

where sign function $\mathrm{sign}(t)$ equals -1 when $t < 0$ and equals 1 when $t > 0$.

By taking Fourier transform of (21), we can obtain the impulse response of $h(t)$ in frequency domain with a complex function

$$H(\omega) = F\{h(t)\} = H_{\mathrm{real}}(\omega) + jH_{\mathrm{imag}}(\omega) \tag{22}$$

with

$$H_{\mathrm{real}}(\omega) = \frac{2}{\pi}\int_0^{\infty} \frac{\omega' H_{\mathrm{imag}}(\omega')}{\omega'^2 - \omega^2} d\omega' \tag{23}$$

$$H_{\mathrm{imag}}(\omega) = -\frac{2\omega}{\pi}\int_0^{\infty} \frac{H_{\mathrm{real}}(\omega')}{\omega'^2 - \omega^2} d\omega'. \tag{24}$$

Here, $H_{\mathrm{real}}(\omega)$ and $H_{\mathrm{imag}}(\omega)$ are the coefficients of real and imaginary parts of $H(\omega)$, respectively, which are both real numbers. Equation (20) is also addressed as Kramers–Kronig relation or Hilbert transform [17]. Note that (23) and (24) are bidirectional equations, which reveal the dependency of real and imaginary part of impulse response, and also provide a necessary and sufficient condition for a causal LTI system.

Note that the causality of a LTI system can be enforced by correcting the real or imaginary part in (23) and (24) with truncation. However, truncation error could be also introduced with largely reduced accuracy for simulation.

One criteria to verify causality by tabulated S-parameters is to measure the error difference (e_{ij}) between imaginary part and its Hilbert transform of real part

$$e_{ij}(\omega_n) = |\mathrm{Hilbert}\{\mathrm{Real}[S_{ij}(\omega_n)]\} - \mathrm{Imag}[S_{ij}(\omega_n)]|. \tag{25}$$

Whether a system is causal or noncausal is determined by the error threshold that can be tolerated in the numerical analysis [38]. A smaller e_{ij} is usually desired to ensure the accuracy and the convergence in simulation.

A flow of causality verification and enforcement is illustrated in Fig. 3. Firstly, a very wide band initial tabulated S-parameter needs to be generated by numerical calculation from the model under investigation. Secondly, both the real and imaginary parts are extracted, and Hilbert transform is applied to the real parts according to (24). Finally, the causality is verified by calculating e_{ij} from (25); and enforced by replacing the imaginary part of

the original tabulated data with the Hilbert transform of the real part in the frequency band of interest. Note that the bandwidth of initial data must be much larger than the final frequency band after causality enforcement to minimize reconstruction and discretization errors [39].

C. Causality of T-Line Model

The relationship between real and imaginary parts in (23) and (24) also relates the amplitude and phase. Provided the magnitude, one can calculate the phase and vice versa. According to the theory of linear system, any causal and stable impulse response $H(\omega)$ can be decomposed into the production of the minimum phase function and all-pass function [40] by

$$H(\omega) = H_{\min}(\omega) \cdot H_{\text{all}}(\omega) \tag{26}$$

where $H_{\min}(\omega)$ and $H_{\text{all}}(\omega)$ are the minimum phase function and all-pass function, respectively. Since $H_{\text{all}}(\omega)$ does not contain any magnitude information, the system causality can also be ensured if it satisfies the minimum phase function defined by the following condition [41], [42]

$$\lim_{\omega\to\infty}\left(\frac{\gamma(\omega)}{j\omega}\right) \Rightarrow 0. \tag{27}$$

For T-line, the minimum phase function can be calculated by substituting (13) into (27) as

$$\lim_{\omega\to\infty}\left(\frac{\gamma(\omega)}{j\omega}\right) = \lim_{\omega\to\infty}\left[\omega^{\left(\frac{\alpha_L+\alpha_C}{2}-1\right)}\cdot\sqrt{L'C'}\right.$$
$$\left.\cdot\left(\sin\frac{(\alpha_L+\alpha_C)\,\pi}{4} - j\cdot\cos\frac{(\alpha_L+\alpha_C)\,\pi}{4}\right)\right]. \tag{28}$$

We can observe that (28) shows very different responses for fractional-order and integer-order T-line models. For the fractional-order model, (28) equals zero when $\alpha_L+\alpha_C<2$. So the causality is always ensured as the minimum phase function condition when (27) is satisfied. On the other hand, α_L and α_C are both equal to one for the integer-order T-line model, and (28) results in a constant value of $\sqrt{L'C'}$, where L' and C' become the normal inductance and capacitance, respectively. Thus the minimum phase function condition in (27) is violated and model becomes noncausal.

Note that the major reason of noncausal issue in the traditional integer T-line model is due to the linear frequency dependence of the propagation constant $\gamma(\omega)$ when $\alpha_L+\alpha_C=2$ in (13). This cannot model the dispersion loss and nonquasi-static effects in the high frequency application like THz. The reality of integer-order T-line model is lost in THz region, and so is the causality. In contrast the nonideal effects are considered in the proposed fractional-order T-line model by fractional-order dispersion terms, which can largely improve the model reality. As such, both the model accuracy and causality are improved. The causality of the fractional-order model can also be verified in numerical calculation by computing the error terms in (30), which will be discussed in the following section.

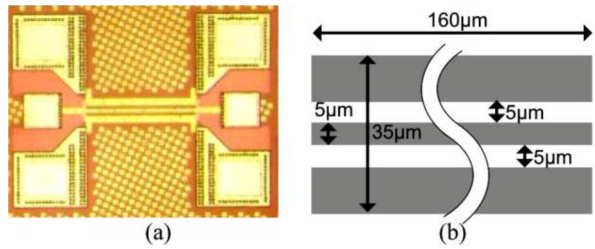

Fig. 4. (a) Die photo of T-line. (b) Dimensions of T-line.

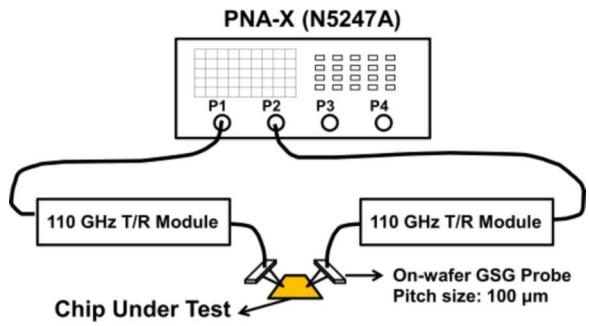

Fig. 5. Measurement setup of on-wafer S-parameter testing up to 110 GHz.

TABLE I
MODELING PARAMETERS OF INTEGER-ORDER AND FRACTIONAL-ORDER RLGC MODEL FOR T-LINE

INTEGER-ORDER MODEL			FRACTIONAL-ORDER MODEL		
PARAMETER	VALUE	UNIT	PARAMETER	VALUE	UNIT
L	247.5	nH/m	α_L	0.862	-
C	0.188	nF/m	L'	10022	$Vs^{-\alpha_L}A^{-1}/m$
R	1200	Ω/m	α_C	0.988	-
R_S	12.56	mΩ/m·rad$^{0.5}$	C'	0.278	$As^{-\alpha_C}V^{-1}/m$
G	0.079	S/m	R	1200	Ω/m
G_D	19.33	pS/m·rad	G	0.079	S/m

IV. T-LINE FRACTIONAL-ORDER MODEL VERIFICATION

A. Extraction From Measurement

As shown in Fig. 4(a), a coplanar waveguide transmission line (CPW-TL) testing structure with RF-PADs is fabricated with Global Foundry 1P8M 65 nm CMOS process, of which the dimensions are given in Fig. 4(b). The CPW-TL is implemented on the top most metal layer with thickness of 3.3 μm. It is measured on CASCADE Microtech Elite-300 probe station by Agilent PNA-X (N5247A) with frequency sweep up to 110 GHz. The measurement setup of S-parameters up to 110 GHz is illustrated in Fig. 5. The reference plane of PNA is calibrated to the ends of GSG probes by SOLT method. Note that both the probes and the impedance standard substrate are provided by Cascade Microtech. RF-PADs on both sides are de-embedded from the measurement results with "open-short" method. Table I summarizes extracted model parameters of both integer-order and fractional-order models based on measurement results. The parameters of traditional integer-order model are extracted according to the procedure by [35]. The parameters of fractional-order model are extracted according to Section III-A.

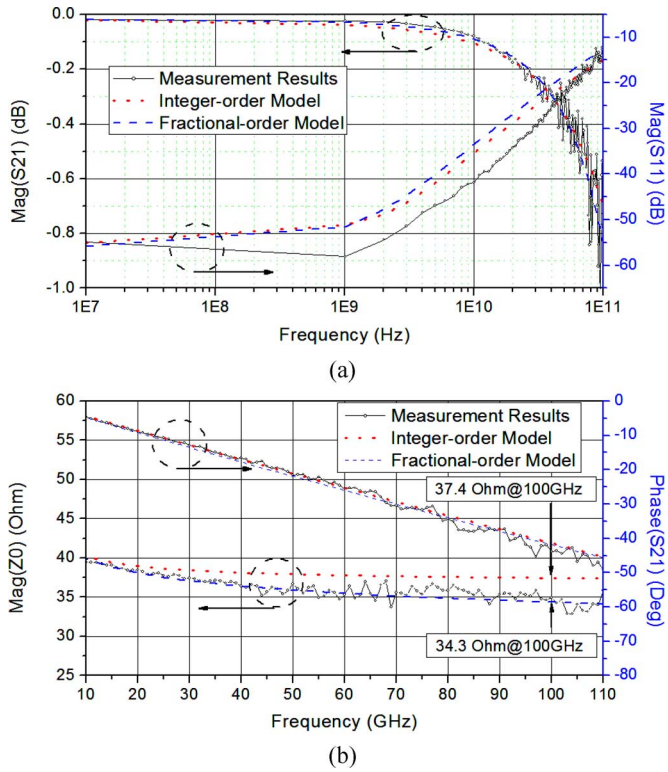

Fig. 6. Verification of fractional-order T-line model with measurement results: (a) magnitude of S11 and S21 in dB, (b) phase delay of S21 and characteristic impedance.

The resulting S-parameters and characteristic impedance (Z_0) of integer-order and fractional-order RLGC models are compared in Fig. 6(b). We can observe that both the traditional integer-order model and the proposed fractional-order model can fit the measurement results in magnitude in Fig. 6(a). Here, a relatively large deviation is observed in magnitude of S11 between the simulation and measurement results. This deviation comes from the equipment noise and calibration error, which is unavoidable as the absolute magnitude of S11 is small ($-15 \sim 50$ dB). Moreover, the phase delay of both traditional integer-order model and the proposed fractional-order model agree well with the measurement results, as shown in Fig. 6(b). However, it is observed that characteristic impedance Z_0 in the traditional integer-order RLGC model has deviated from measurement results above 10 GHz, and almost approaches a constant above 40 GHz. On the other hand, the fractional-order RLGC model closely fits the measured Z_0 up to 110 GHz, because it can accurately consider frequency-dependence loss yet in a compact RLGC form. At 100 GHz, the Z_0 from fractional-order and measurement results are 34.3 Ω, which is 3.1 Ω lower than the one from integer-order model. Note that such difference will keep increasing with frequency and largely affects the model accuracy in traditional integer-order T-line model at THz.

Physically, the values of fractional-order terms (α_L and α_C) model the frequency-dependent dispersion loss of device at THz. For the T-line fabricated by on-chip CMOS process, larger loss is observed in metal layer than in dielectric layer. As a result, α_L has a relatively large deviation from 1, while α_C is close to 1. But note that a slight change in the order-terms (α_L and α_C) could bring huge changes in the prefactors (L' and C') in THz region as observed in (7) and (8).

B. Causality Verification and Comparison

The causality of the proposed fractional-order T-line model can be verified by comparing imaginary parts of S-parameters with the Hilbert transform of real parts. Then, the error term $\mathrm{e}_{ij}(\omega_\mathrm{n})$ is calculated by (30) as discussed in Section III. For the purpose of comparison, the causality of traditional integer-order T-line model is also verified in the same way. The tabulated results for both models are obtained by two-port S-parameter simulation in Agilent Advanced Design System (ADS) based on the extracted model parameters shown in Table I. For a two-port network, four sets of complex S-parameter results can be obtained including S11, S22, S12, and S21. However, according to the reciprocal property of T-line structure ($\mathrm{S11} = \mathrm{S22}$ and $\mathrm{S12} = \mathrm{S21}$), only S11 and S21 are considered in the causality analysis. In order to minimize reconstruction and discretization errors [39] introduced by finite spectrum, the S-parameter simulation is conducted from 0 Hz to 20 THz with a step size of 1 GHz.

Firstly, the causality of return loss (S11) is verified for both integer and fractional order T-line models Fig. 7(a) and (b) shows the comparison between Imag(S11) and the value obtained by Hilbert transformation from real part $\mathrm{Hibert}\{\mathrm{Real(S11)}\}$ for both integer-order and the proposed fractional-order T-line models in the frequency range of 1 GHz–1 THz, respectively. For the traditional integer-order RLCG T-line model, the Imag(S11) starts to deviate from the causal response at 10 GHz and shows large deviation from 100 GHz up to 1 THz as depicted in Fig. 7(a). But for the proposed fractional-order T-line model as shown in Fig. 7(b), we can observe that the Imag(S11) closely fits the causal response obtained from Hibert transformation ($\mathrm{Hibert}\{\mathrm{Real(S11)}\}$). The error magnitude of Imag(S11) from both models are compared in Fig. 7(c), where a dramatic error reduction is observed by the application of fraction order T-line model. Note that the error magnitude is calculated by

$$e_{11} = |\mathrm{Hilbert}\{\mathrm{Real}(S11)\} - \mathrm{Imag(S11)}|. \tag{29}$$

Secondly, the causality of return loss (S21) is verified for both integer and fractional order T-line model. The comparison between Imag(S21) and causal response for both models are illustrated in Fig. 7(d) and (e). For the traditional integer-order RLCG T-line model, the Imag(S21) obtained from the integer-order RLCG T-line model deviates from the causal response (1–10 GHz) as depicted in Fig. 7(d). But for the proposed fractional-order T-line model as shown in Fig. 7(e), we can observe that the Imag(S21) of the fractional-order T-line model closely fits the causal response. A clear comparison by error magnitude of Imag(S21) from both modelsis illustrated in Fig. 7(f), where a dramatic error reduction is also observed by the proposed fractional-order T-line model. Note that the error magnitude is calculated by

$$e_{21} = |\mathrm{Hilbert}\{\mathrm{Real}(S21)\} - \mathrm{Imag}(S21)|. \tag{30}$$

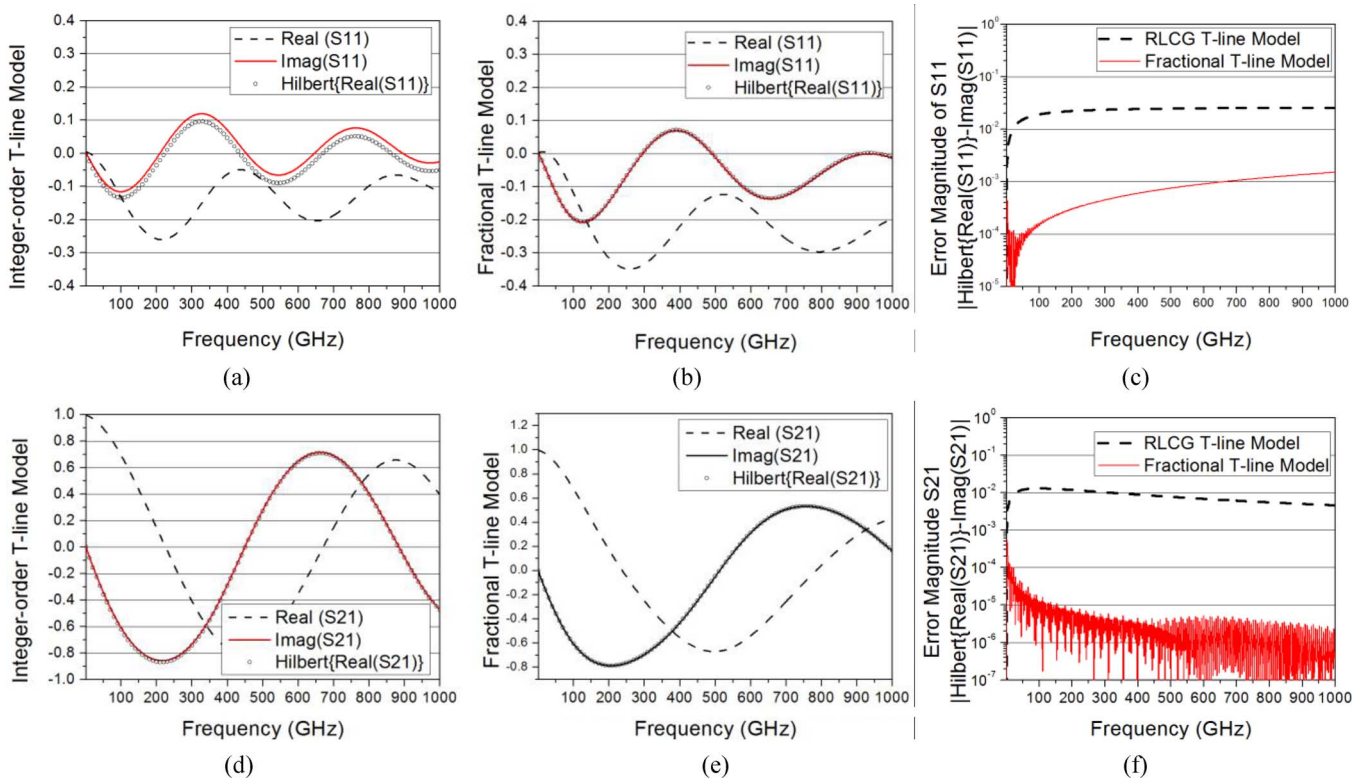

Fig. 7. Causality verification by Hilbert transformation for both integer and fractional order T-line models: (a) integer-order T-line model S11; (b) fractional-order T-line model S11; (c) error magnitude comparison of S11; (d) integer-order T-line model S21; (e) fractional-order T-line model S21; and (f) error magnitude comparison of S21.

Note that since both e_{11} and e_{21} for fractional-order T-line model are rather small, the causality enforcement by (23) and (24) is not required. The resulting frequency model can be directly used to estimate the time-domain model by the rational fitting. As such, the best accuracy could be ensured in the time-domain simulation such as Transient Analysis or Periodic Steady State (PSS) Analysis. But for the traditional integer-order RLCG T-line model, the noncausal effect could have convergence issues. One way to alleviate the causality issue of the integer-order RLCG T-line model is by truncating the model data with the causality enforcement, but the accuracy is lost in this way as discussed in Section III-B. Such issues will be further evaluated in the following section for design and analysis of CMOS-based THz integrated circuits.

V. T-Line Fractional-Order Model Application

After verified and correlated with measurement results, we further study the impact of the proposed fractional-order T-line model to the design of CMOS based THz integrated circuits. T-line is not only commonly used as wide band interconnect, but also can be utilized in circuit components. In this section, the impact to apply the proposed fractional-order T-line model is evaluated by the circuit level design and analysis with comparison to the traditional integer-order T-line model. Firstly, we study the T-line impulse response. Secondly, a quarter-wavelength $(\lambda/4)$ T-line is applied as the short circuit for the local oscillation signal in a down conversion mixer; and lastly, T-line is applied as the resonator in the design of one standing wave oscillator.

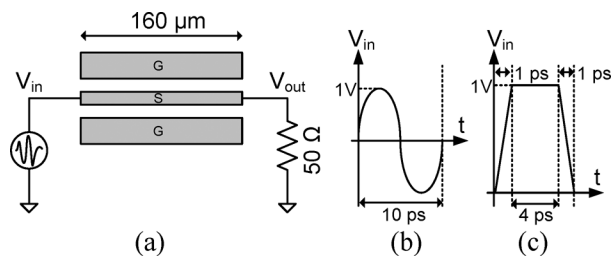

Fig. 8. (a) Schematic of T-line impulse response simulation. (b) Waveform of sinusoidal input. (c) Waveform of trapezoidal input.

A. T-Line Impulse Response

Signal integrity is important when T-line is deployed as interconnect to integrate different modules in THz integrated circuits. An accurate T-line model can help predict the signal delay, attenuation, overshoot, as well as dispersion, which are all key performance indicators that can be inferred from the impulse response. We compare the impulse responses of the proposed fractional-order T-line model and the traditional integer-order model in this part. As shown in Fig. 8(a), the input of a 160 μ m coplanar waveguide T-line is excited by an input of voltage source with arbitrary waveform on the left-hand side, and its output is terminated by a 50 Ω resistance on the right-hand side. The modeling parameters of this T-line are obtained from Table I, and are deployed in transient analysis in Cadence Spectre simulator. The fractional-order model, integer-order model and integer-order model after causality enforcement are deployed, as discussed in Section III-B. Note

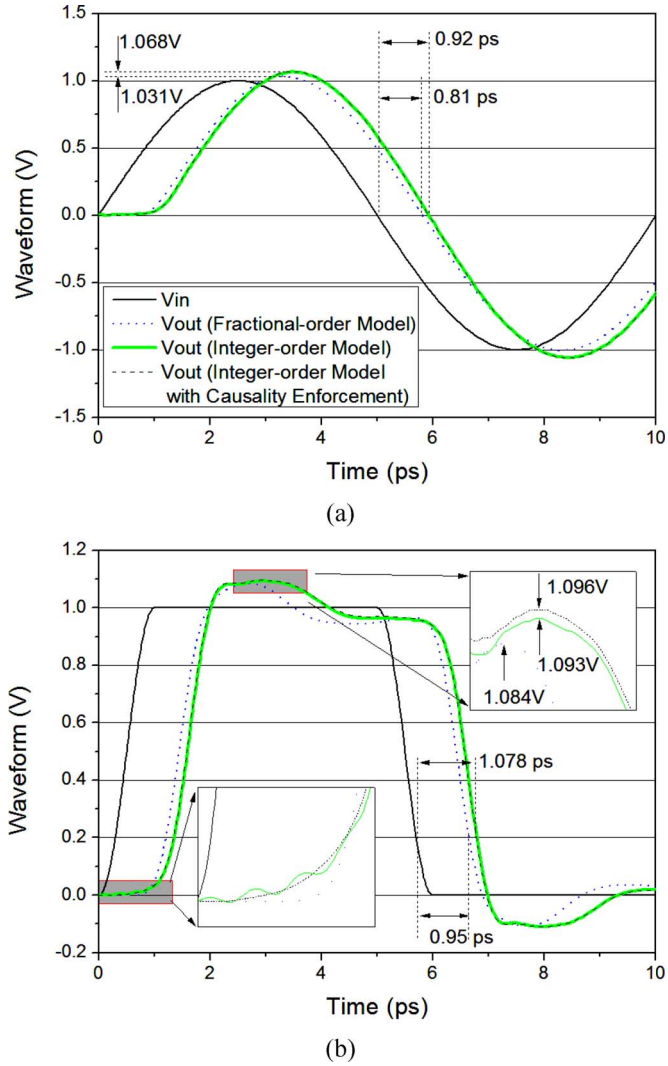

Fig. 9. Impulse responses of T-line models under different input waveforms: (a) sinusoidal input, (b) piecewise-Linear input.

that the frequency domain models are transferred to time-domain models by the rational fitting method with the rational order of 19 and maximum absolute error of 0.001, as discussed in Section III-C.

1) Sinusoidal Input: A sinusoidal input with amplitude of 1 V and frequency of 100 GHz is applied shown in Fig. 8(b). The impulse response of T-line is illustrated in Fig. 9(a). We can observe that the signal delay from the fractional-order model is only 0.81 ps, which is 12% less than the values obtained from the integer-order model and the one with causality enforcement. This is a direct consequence of the overestimated T-line characteristic impedance by the integer-order T-line models. We know that the signal delay is increased with the product of distributed inductance and capacitance [43] . The delay from the integer-order model is higher because of the overestimated distributed inductance as well as the characteristic impedance (Z_0) at high-frequency region. In contrast, in the fractional-order model, the distributed inductance is modeled with reduction due to the nonquasi-static effect at very high frequency such that the signal delay is smaller. Accordingly, the energy loss is increased due to the inductance reduction. As such, the amplitude obtained from the fractional-order model is 1.031 V, which is lower than that of the one (1.068 V) from the integer-order model by 0.037 V. Note that 12% delay error could be very severe, as it will be scaled with the length of T-line in the real application.

2) Piecewise-Linear Input: A trapezoidal-typed piecewise-linear input is applied as shown in Fig. 8(c), which has magnitude between 0 and 1 V, pulse-width of 4 ps and rise/fall time of 1 ps. Its impulse response is illustrated in Fig. 9(b). Unlike the sinusoidal signal with single frequency spectrum, a trapezoidal waveform has spread spectrum. Therefore, it usually suffers the dispersion effect during the signal propagation, which means unequal phase velocities of signals at different frequencies. Such effect is monitored from the simulation results where the corners of the original input waveform are rounded at output. We can observe that the transition between 0 and 1 V with the fractional-order model is much smoother than the one by the integer-model model due to a better modeling for the dispersion effect.

The signal delay from the fractional-order model is 0.95 ps, which is also 12% less than the value obtained from the integer-order model. One can also observe that the signal delay from the trapezoidal input is around 14% higher than the sinusoidal input. This is mainly due to the reduction of phase velocity in higher frequency region. Moreover, it is interesting to monitor a noncausal effect from the integer-order model at the time around 1 ps as enlarged in Fig. 9(b), where the output signal tends to rise before the input signal arrives. Note that in a causal system, the output signal should not change before the input signal arrives. In the case of T-line, the output signal should not change immediately after the input due to the delay of the signal propagation. Obviously, the output signal from the integer-order T-line model contradicts this principle of causality. On the other hand, such a noncausal effect is not observed when using the proposed fractional-order model. In addition, due to the modeling of energy loss by the inductance reduction, indicated from the fractional-order model, the peak voltage from the fractional-order model is 1.084 V, which is lower than that of the integer-order model by 0.009 V. It is also found that the causality enforcement will reduce the model accuracy by further increasing the peak voltage to 1.096 V.

B. Single-Gate Mixer With $\lambda/4$ T-Line Stub

The other design example is to use T-line as the $\lambda/4$ AC ground in the mixer design. An open-ended $\lambda/4$ T-line is connected to a signal trace to form LO short at the mixer output. Note that an accurate T-line model can help predict the rejection ratio of LO-signal and the conversion gain at output.

As shown in Fig. 10, a single-gate mixer [44] is designed for down converting a 95–105 GHz signal to 20–30 GHz by a 75 GHz LO-signal. The mixer is constructed by a common source NMOS transistor and a drain connected 200-Ω resistor. The NMOS transistor has the width of 30 μm and length of 60 nm, of which the model is obtained from Global Foundry 65 nm CMOS library. A $\lambda/4$ T-line stubis connected to the mixer output to reject the LO-signal, of which the modeling parameters are still obtained from Table I. The T-line models are scaled

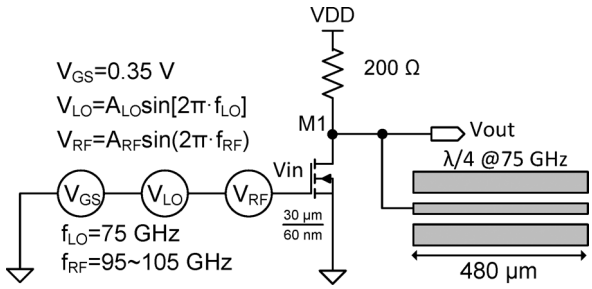

Fig. 10. Schematic of single-gate mixer with $\lambda/4$ T-line stub.

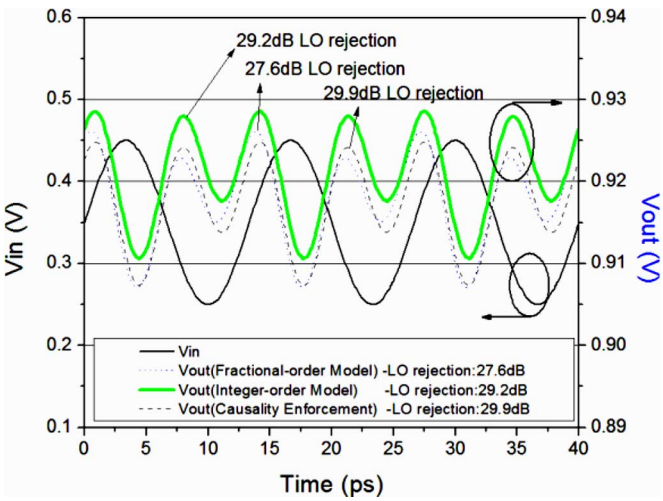

Fig. 11. LO-rejection effect of open ended $\lambda/4$ T-line in single-gate mixer.

to the length of 480 μm to become a $\lambda/4$ at 75 GHz. The mixer operates under 1 V power supply, and the transistor is biased at sub-threshold region with V_{GS} of 0.35 V. The circuit analysis of mixer is conducted with Cadence Spectre simulator in two steps for different T-line models. Firstly, the LO-rejection performance is studied by PSS analysis. Secondly, the conversion gain of mixer is evaluated by PSS and Periodic AC (PAC) analysis.

1) LO Rejection: In order to compare the performance of LO-rejection by the two $\lambda/4$ T-line models, a relatively small LO-signal ($A_{LO} = 0.1$ V) without RF signal ($A_{RF} = 0$ V) is applied to the mixer input. As shown in the time-domain simulation results in Fig. 11, the 75 GHz LO-signal almost disappears at the output for T-line models and its second harmonic at 150 GHz becomes more dominant. A numerical calculation shows that the LO-rejection from the fractional-order T-line model is 27.6 dB, which is 1.6 dB lower than that from the integer-order model and is 2.3 dB lower than that from the inter-order model with causality enforcement. We know that the rejection ratio of the $\lambda/4$ T-line open-stub is determined by cancellation of the incident wave and reflected wave at the connecting point of T-line. Compared to the traditional integer-order model, the fractional-order model can accurately consider the additional energy loss from the nonquasi-state effect at 75 GHz and hence predicts a smaller reflected wave with a lower level rejection. We can also observe that the causality enforcement does not help improve the accuracy in this case.

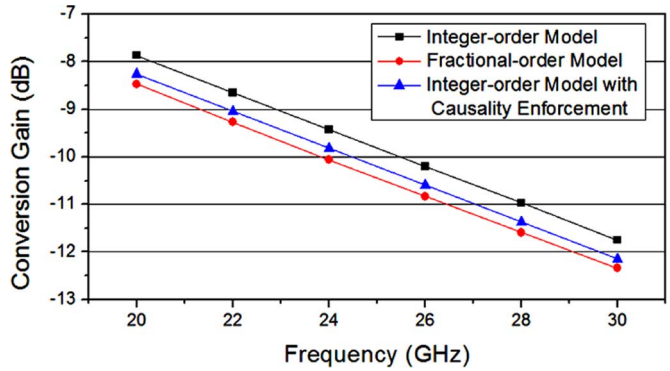

Fig. 12. Conversion gain of mixer when input signal at 95–105 GHz down converted to 20–30 GHz with LO frequency of 75 GHz.

2) Conversion Gain: The mixer conversion gain is then simulated when a relatively large LO amplitude ($A_{LO} = 0.6$ V) and a small RF signal ($A_{RF} = 0.1$ V) are applied to the mixer input. As shown by the simulation results in Fig. 12, the conversion gain obtained from the fractional order T-line model is about 0.6 dB lower than that from the integer-order model and 0.2 dB lower than the one after causality enforcement. The output frequency range is of 20–30 GHz. Note that the conversion gain is not related to the T-line model directly, but from the power level of LO-signal. As discussed in the last section, LO-rejection is reduced by a lossy $\lambda/4$ T-line. Thus, the LO power applied to the mixer is reduced accordingly, which in turn reduces the conversion efficiency. Here, we can conclude that the fractional-order model can accurately consider this loss but the integer-order model even with the causality enforcement cannot produce an accurate estimation of the conversion gain.

C. Standing-Wave Oscillator With CPW T-Line Resonator

T-line can be also applied as the resonator in the standing-wave oscillator design [45]. Unlike the short circuit created by open-ended $\lambda/4$ T-line discussed in the last section, T-line resonator forms a very high impedance at the oscillation frequency with sharp frequency response. So the oscillation can be sustained if sufficient energy compensation is provided. Here, an accurate T-line model can help predict the true performance of oscillator including settling time, oscillation amplitude, oscillation frequency, as well as the phase noise. As such, a standing-wave oscillator around 10 GHz is designed with CPW-TL structure to further demonstrate the advantage of the proposed fractional-order T-line model at THz.

As shown in Fig. 13, a standing-wave resonator is formed by differential CPW-TL structure, of which the modeling parameters are still from Table I. Oscillator is designed by connecting the CPW T-line resonator with a negative resistance, which is formed by crosscoupled NMOS transistors from the GF 65 nm CMOS library. Both NMOS transistors are identical to each other with the width of 24 μm and length of 60 nm. The oscillator operates under 1 V power supply and the tail current is provided by a constant current source of 5 mA. The circuit analysis of oscillator is conducted with Cadence Spectre simulator in two steps for different T-line models. Firstly, the oscillation amplitude and settling time are studied by transient anal-

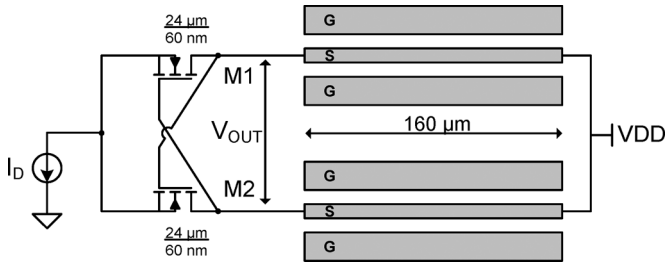

Fig. 13. Schematic of standing-wave oscillator with CPW T-line.

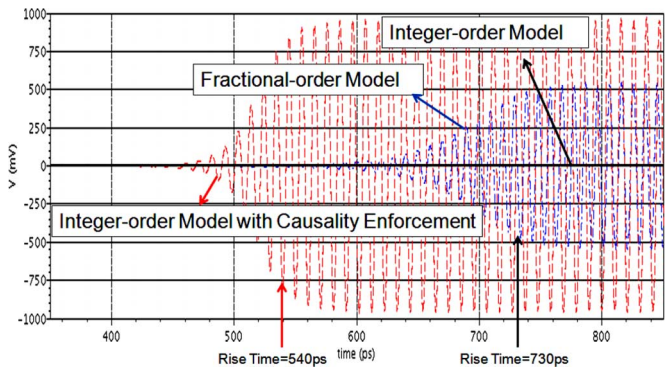

Fig. 14. V_{OUT} transient response of standing-wave oscillators with T-line modeled by r fractional-order and integer-order models.

ysis. Secondly, the phase noise of oscillator is evaluated by PSS analysis.

1) Oscillation Amplitude and Settling Time: After oscillator is powered up, the oscillation signal starts to build up from noise level and quickly reaches its maximum amplitude. This transient response of V_{OUT} is illustrated in Fig. 14. One interesting observation is that the oscillator with the integer-order T-line model cannot start oscillation due to the causality issue. Not until the model is fixed by the integer-order model with the causality enforcement, the oscillation signal can be then observed. As such, we can only compare the simulation results between the fraction-order model and the integer-order model after causality enforcement.

The oscillation frequency with the fractional-order T-line model is 103.4 GHz. Due to the deviation in the characteristic impedance, the oscillator with the integer-order model after causality enforcement oscillates at a different frequency of 96.6 GHz. The simulated settling time of oscillator with the fractional-order T-line is 730 ps, which is 190 ps longer than the value from the corrected integer-order model. It is known that the settling time is related to the damping factor of transfer function [46]. Due to the additional loss introduced at around 100 GHz by the nonquasi-static effect, the damping factor is increased and resulting in a longer settling time, which can be predicted by the proposed fractional-order model. Moreover, this additional energy loss also limits the maximum oscillation amplitude. We can see that the stabilized amplitude from the fraction-order mode is 550 mV, which is almost 400 mV less than that from the corrected integer-order model.

2) Oscillation Frequency and Phase Noise: The quality factor (Q) of the T-line resonator will also be reduced by the additional energy loss introduced by the nonquasi-static effect,

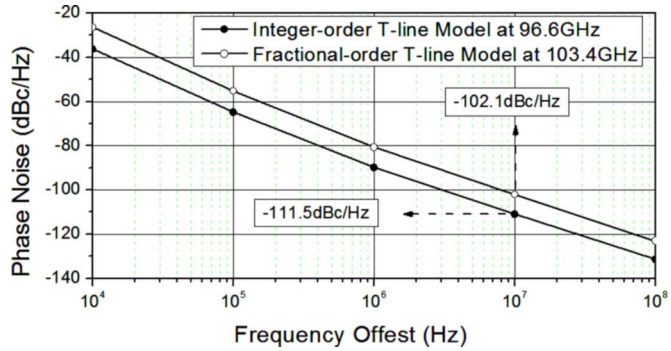

Fig. 15. Phase noise of standing-wave oscillators with T-line modeled the fractional-order and integer-order models.

which further affects the phase noise of oscillator. As shown in Fig. 15, the phase noise obtained from the fractional-order T-line model at 103.4 GHz is 9.4 dB worse than the corrected integer-order model at 96.6 GHz

VI. Conclusion

Accurate device model is critical for CMOS based THz circuit design. Since transmission line (T-line) is one of the most fundamental passive devices commonly used in the THz circuit design, an in-depth study of T-line model at THz is thereby important. Note that dispersion and nonquasi-static effects are difficult to be modeled by traditional methods such as the integer-order RLCG model with causality. In this paper, a compact and causal fractional-order RLGC model for T-line is proposed to solve the causality concern and to consider the frequency-dependent dispersion loss and nonquasi-static effect at THz.

The measured results have confirmed that the proposed fractional-order RLGC model has improved accuracy over the traditional integer-order RLGC model beyond 10 GHz. Accordingly, the proposed fractional-order T-line model can be applied in the design and analysis for CMOS based THz circuits. As illustrated by a number of circuit design examples including T-line with impulse response, mixer, and oscillator, the use of the proposed fractional-order T-line model can improve the simulation accuracy with no causality-caused convergence issues.

Acknowledgment

The authors appreciate the measurement support by W.-M. Lim at VIRTUS IC Design Centre of Excellence, Nanyang Technological University, Singapore.

References

[1] C. Yu, S. Fan, Y. Sun, and E. Pickwell-MacPherson, "The potential of terahertz imaging for cancer diagnosis: A review of investigations to date," *Quant. Imag. Med. Surg.*, vol. 2, no. 1, pp. 33–45, Mar. 2013.

[2] P. C. Ashworth, E. Pickwell-MacPherson, E. Provenzano, S. E. Pinder, A. D. Purushotham, M. Pepper, and V. P. Wallace, "Terahertz pulsed spectroscopy of freshly excised human breast cancer," *Opt. Exp.*, vol. 17, no. 15, pp. 12444–12454, Jul. 2009.

[3] D. Cai, Y. Shang, H. Yu, and J. Ren, "An 80 GHz on-chip metamaterial resonator by differential transmission line loaded with split ring resonator," *IET Electron. Lett.*, vol. 48, no. 18, pp. 1128–1130, Aug. 2012.

[4] W. Fei, H. Yu, Y. Shang, and K. S. Yeo, "A 2D distributed power combining by metamaterial-based zero-phase-shifter for 60 GHz power amplifier in 65 nm CMOS," *IEEE Trans. Microw. Theory Tech.*, vol. 61, no. 1, pp. 505–516, Jan. 2013.
[5] W. Fei, H. Yu, Y. Shang, D. Cai, and J. Ren, "A 96 GHz oscillator by high-Q differential transmission line loaded with complementary split ring resonator in 65 nm CMOS," *IEEE Trans. Circuits Syst. II*, vol. 60, no. 3, pp. 127–131, Mar. 2013.
[6] Y. Shang, H. Yu, D. Cai, J. Ren, and K. S. Yeo, "Design of high-Q millimeter-wave oscillator by differential transmission line loaded with metamaterial resonator in 65 nm CMOS," *IEEE Trans. Microwave Theory Tech.*, vol. 61, no. 5, pp. 1892–1902, May 2013.
[7] T. Cisse Haba, G. Ablart, T. Camps, and F. Oliviec, "Influence of the electrical parameters on the input impedance of a fractal structure realised on silicon," *Chaos, Solitons Fractals*, vol. 24, no. 2, pp. 479–490, Apr. 2005.
[8] T. Cisse Haba, G. L. Loum, and G. Ablart, "An analytical expression for the input impedance of a fractal tree obtained by a microelectronical process and experimental measurements of its non-integral dimension," *Chaos, Solitons Fractals*, vol. 33, no. 2, pp. 364–373, Jul. 2007.
[9] Y. Shang, D. Cai, W. Fei, H. Yu, and J. Ren, "An 8 mW ultra low power 60 GHz direct-conversion receiver with 55 dB gain and 4.9 dB noise figure in 65 nm CMOS," in *IEEE Int. Symp. Radio-Freq. Integrat. Technol.*, Nov. 2012., pp. 47–49.
[10] D. Cai, H. Fu, J. Ren, W. Li, N. Li, H. Yu, and K. S. Yeo, "A dividerless PLL with low power and low reference spur by aperture-phase detector and phase-to-analog converter," *IEEE Trans. Circuits Syst. I*, vol. 60, no. 1, pp. 37–50, Jan. 2013.
[11] Y. Shang, H. Fu, H. Yu, and J. Ren, "A 78 dBm Sensitivity 96 GHz super-regenerative receiver with quench-controlled metamaterial oscillator in 65 nm CMOS," in *Proc. IEEE Radio-Freq. Integrat. Circuits Symp.* , Jun. 2013, pp. 447–450.
[12] W. Fei, H. Yu, W. M. Lim, and J. Ren, "A 53-to-73 GHz power amplifier with 74.5mW/mm2 output power density by 2D differential power combining in 65nm CMOS," in *Proc. IEEE Radio-Freq. Integrat. Circuits Symp.*, Jun. 2013, pp. 271–274.
[13] *"Star-HSPICE Manual,"* HSPICE, Fremont, CA, Jan. 2001, ch.18.
[14] Modeling Coilcraft RF Inductors, Document 158, Jul. 2, 2001 [Online]. Available: http://www.coilcraft.com/
[15] C.-S. Yen, Z. Fazarinc, and R. L. Wheeler, "Time-domain skin-effect model for transient analysis of lossy transmission lines," *Proc. IEEE*, vol. 70, no. 7, pp. 750–757, Jul. 1982.
[16] S. Cho, K. R. Kim, B.-G. Park, and I. M. Kang, "Non-quasi-static modeling of silicon nanowire metal-oxide-semiconductor field-effect transistor and its model verification up to 1 THz," *Jpn. J. Appl. Phys.*, vol. 49, p. 110206, Nov. 2010.
[17] J. Bechhoefer, "Kramers-Kronig, Bode, and the meaning of zero," *Am. J. Phys.*, vol. 79, no. 10, pp. 1053–1059, Oct. 2011.
[18] S. Westerlund and L. Ekstam, "Capacitor theory," *IEEE Trans. Dielectr. Electr. Insulat.*, vol. 1, no. 4, pp. 826–839, Oct. 1994.
[19] I. Schäfer and K. Krüger, "Modelling of lossy coils using fractional derivatives," *J. Phys. D: Appl. Phys.*, vol. 41, p. 045001, Jan. 2008.
[20] Y. Shang, W. Fei, and H. Yu, "A fractional-order RLGC model for terahertz transmission line," in *IEEE Int. Microw. Symp.*, Jun. 2013.
[21] J. Lanoë, S. Le Maguer, and M. M. Ney, "A fractional derivative operator for surface impedance TLM modeling," in *IEEE Microw. Wireless Compon. Lett.*, Sep. 2007, vol. 17, no. 9, pp. 625–627.
[22] Y. Zhang and D. Xue, "Modeling and simulating transmission lines using fractional calculus," in *Int. Conf. Wireless Commun., Network. Mobile Comput. (WiCOM)*, Sep. 2007, pp. 3115–3118.
[23] A. Shamim, A. G. Radwan, and K. N. Salama, "Fractional smith chart theory," in *IEEE Microw. Wireless Compon. Lett.*, Mar. 2011, vol. 21, no. 3, pp. 117–119.
[24] A. G. Radwan, A. Shamim, and K. N. Salama, "Theory of fractional order elements based impedance matching networks," *IEEE Microw. Wireless Compon. Lett.*, vol. 21, no. 3, pp. 120–122, Mar. 2011.
[25] A. G. Radwan and K. N. Salama, "Passive and active elements using fractional LβCα circuit," *IEEE Trans. Circuits Syst. I, Reg. Papers*, vol. 58, no. 10, pp. 2388–2397, Oct. 2011.
[26] A. S. Elwakil, "Fractional-order circuits and systems: An emerging interdisciplinary research area," *IEEE Circuits Syst. Mag.*, vol. 10, no. 4, pp. 40–50, 2010.
[27] J. C. Wang, "Realizations of generalized Warburg impedance with RC ladder networks and transmission lines," *J. Electrochem. Soc.*, vol. 134, no. 8, pp. 1915–1920, 1987.
[28] N. Engheta, "On the role of fractional calculus in electromagnetic theory," *IEEE Antennas Propag. Mag.*, vol. 39, no. 4, pp. 35–46, Aug. 1997.
[29] S. W. Wheatcraft and M. M. Meerschaert, "Fractional conservation of mass," *Adv. Water Resources*, vol. 31, no. 10, pp. 1377–1381, Oct. 2008.
[30] B. Nolte, S. Kempfle, and I. Schäfer, "Does a real material behave fractionally? Applications of fractional differential operators to the damped structure borne sound in viscoelastic solids," *J. Computat. Acoust.*, vol. 11, no. 3, p. 451, 2003.
[31] N. Laskin, "Fractional quantum mechanics and levy path integrals," *Phys. Lett. A*, vol. A268, pp. 298–305, 2000.
[32] M. A. E. Herzallah and D. Baleanu, "Fractional-order Euler-Lagrange equations and formulation of Hamiltonian equations," *Nonlinear Dynam.*, vol. 58, no. 1–2, pp. 385–391, Oct. 2009.
[33] I. Petráš, *Fractional-Order Nonlinear Systems, Modeling, Analysis and Simulation*. New York: Springer, 2011.
[34] J. Zhang, J. L. Drewniak, D. J. Pommerenke, M. Y. Koledintseva, R. E. DuBroff, W. Cheng, Z. Yang, Q. B. Chen, and A. Orlandi, "Causal RLGC(f) models for transmission lines from measured S-parameters," *IEEE Trans. Electromagn. Compatibil.*, vol. 52, no. 1, pp. 189–198, Feb. 2010.
[35] M. J. Degerstrom, B. K. Gilbert, and E. S. Daniel, "Accurate resistance, inductance, capacitance, and conductance (RLCG) from uniform transmission line measurements," *IEEE Electrical Performance Electron. Packag.*, pp. 77–80, Oct. 2008.
[36] B. Gustavsen and A. Semlyen, "Rational approximation of frequency domain responses by vector fitting," *IEEE Trans. Power Del.*, vol. 14, no. 3, pp. 1052–1061, Jul. 1999.
[37] M. R. Wohlers, *Lumped and Distributed Passive Networks*. New York: Academic, 1969.
[38] V. Lucarini, Y. Ino, K.-E. Peiponen, and M. Kuwata-Gonokami, "Detection and correction of the misplacement error in terahertz spectroscopy by application of singly subtractive Kramers-Kronig relations," *Phys. Rev. B, Condens. Matter*, vol. 72, p. 1251071, 2005.
[39] P. Triverio and S. Grivet-Talocia, "Robust causality characterization via generalized dispersion relations," *IEEE Trans. Adv. Packag.*, vol. 31, no. 3, pp. 579–593, Aug. 2008.
[40] V. Alan, *Oppenheim and Ronald W. Schafer, Discrete-Time Signal Processing*, 3rd ed. Upper Saddle River, NJ: Prentice-Hall, 2009.
[41] H. W. Bode, *Network Analysis and Feedback Amplifier Design*. New York: Van Nostrand, 1945.
[42] N. S. Nahman, "A discussion on the transient analysis of coaxial cables considering high-frequency losses," *IRE Trans. Circuit Theory*, vol. 9, no. 2, pp. 144–152, Jun. 1962.
[43] J. J. Karakash, *Transmission Lines and Filter Networks*. New York: Macmillan, 1950.
[44] S. Emami, C. H. Doan, A. M. Niknejad, and R. W. Brodersen, "A 60-GHz down-converting CMOS single-gate mixer," in *IEEE Radio Freq. Integrat. Circuits Symp.*, Jun. 2005, pp. 163–166.
[45] T. LaRocca, J. Liu, F. Wang, D. Murphy, and F. Chang, "CMOS digital controlled oscillator with embedded DiCAD resonator for 58–64 GHz linear frequency tuning and low phase noise," in *IEEE Int. Microw. Symp.*, 2009, pp. 685–688.
[46] K. Ogata, *Modern Control Engineering*. Upper Saddle River, NJ: Prentice Hall, 2002.

Yang Shang (S'11) received the B.S. and M.S. degree in electrical and electronic engineering both from Nanyang Technological University, Singapore in 2005 and 2009, respectively. He is currently working towards the Ph.D. degree with School of Electrical and Electronics Engineering at Nanyang Technological University. His research interests are Terahertz device model and meta-material for CMOS RF/MMIC.

Hao Yu (M'06) receivedthe B.S. degree from Fudan University, China; and Ph.D. degree from the Electrical Engineering Department, University of California, USA. He was a senior research staff at Berkeley Design Automation. Since October 2009, he has been an Assistant Professor at the School of Electrical and Electronic Engineering, Nanyang Technological University, Singapore. His primary research interests are 3D-IC and RF-IC at nano-tera scale. He has 96 peer-reviewed top-tier publications. Dr. Yu received Best Paper Award from the ACM TODAES'10, Best Paper Award nominations in DAC06, ICCAD'06, ASP-DAC'12, Best Student Paper (advisor) finalist in SiRF'13, RFIC'13, and Inventor Award'08 from semiconductor research cooperation. He is associate editor and technical program committee member for a number of IEEE/ACM journals and conferences.

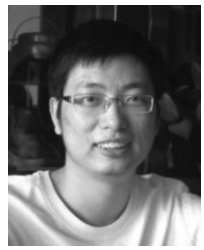

Wei Fei (S'10) received the B.S. degree in electrical and electronic engineering from Nanyang Technological University, Singapore in 2007. He is currently working towards the Ph.D. degree with School of Electrical and Electronic Engineering at Nanyang Technological University. His research interest is to explore CMOS IC design at the extreme scale, including nano-electronics and MMIC at THz.